In: AIAA SCITECH 2024 Forum, 8-12 January 2024, Orlando, FL, USA
DOI:10.2514/6.2024-1616

Design optimisation of separate-jet exhausts with CFD in-the-loop and dimensionality reduction techniques

J. Hueso-Rebassa* ,D. MacManus† , F. Tejero‡ , I. Goulos§
Cranfield University, Cranfield, Bedfordshire, MK43 0AL, United Kingdom

C. Abdessemed¶, C. Sheaf‖
Rolls-Royce plc, Derby, DE24 8BJ, United Kingdom

For Ultra-High Bypass Ratio aero-engines, the exhaust system is likely to play a significant role on the aerodynamics and performance of the aircraft. For this reason, relatively rapid methods for the aerodynamic design and optimisation of exhaust systems are required to inform design decisions at early stages of the design process. Previous exhaust optimisation works encompassed Response Surface Model (RSM) based optimisations of nozzle configurations that were parametrised with a significant number of design variables. The RSM were constructed with a large database of designs that were assessed with fine computational meshes and well resolved boundary layers. However, the large number of design variables and the computational cost required to evaluate each exhaust design limited the optimisation capabilities. This work develops a relatively more rapid exhaust optimisation method based on CFD in-the-loop and dimensionality reduction. The methodology is based on coarse meshes and wall functions to guide the optimisation process and is coupled with methods for the identification of the dominant design variables. For an UHBR aero-engine exhaust design space of 16 design variables, it was found that the velocity coefficient could be characterised with only seven parameters. Based on these results, various optimisation methods were developed and applied. These targeted the maximisation of the velocity coefficient by optimising just the 7 dominant design variables. With these approaches, a similar benefit in exhaust performance relative to the baseline optimisation method was obtained approximately 4 times faster.

I. Introduction

To reduce fuel consumption, the next generation of aero-engine powerplants are likely to operate with higher bypass-ratios (BPR) and lower fan pressure ratios [1]. This will reduce Specific Fuel Consumption (SFC) and improve propulsive efficiency [2, 3]. While current in-service High Bypass Ratio aero-engines are designed with a $BPR > 10$ [4], Ultra-High Bypass Ratio (UHBR) engines are expected to operate with $BPR > 15$ [4, 5]. For UHBR aero-engines, the exhaust system is likely to play a significant role on the aerodynamics and performance of the aircraft [6, 7]. For this reason, relatively rapid methods for the aerodynamic design and optimisation of exhaust systems are required to inform design decisions at early stages of the design process.

Goulos et al. [8–11] developed an integrated design space exploration (DSE) and optimisation framework for two-dimensional axisymmetric separate-jet exhausts. The methodology was based on the genetic algorithm (GA) optimisation of a Kriging RSM constructed from a computational fluid dynamics (CFD) database. It relied on the acquisition of sufficient data to build accurate RSMs. The sampling method was a Latin Hypercube approach [12] which allowed a total of 720 samples to be uniformly spread around a design space of 12 independent design variables [9]. The method was used to optimise the velocity coefficient (C_v) of a Ultra-High Bypass Ratio (UHBR) exhaust system [9]. A benefit of 0.065% on C_v was reported relative to the baseline configuration. The same RSM based optimisation was used to study the effect of the exit flow conditions of the fan Outlet Guide Vanes (OGV) on separate-jet exhausts [11]. The research targeted the optimisation of exhaust geometries together with OGV total pressure (P_t) and total temperature

*Research Fellow in Propulsion Aerodynamics, Propulsion Engineering Centre, Cranfield University, j.hueso-rebassa@cranfield.ac.uk
†Head of Gas Turbine Technology Group, Propulsion Engineering Centre, Cranfield University
‡Lecturer in Propulsion Systems Design, Propulsion Engineering Centre, Cranfield University
§Senior Lecturer in Propulsion Aerodynamics and Performance Engineering, Propulsion Engineering Centre, Cranfield University
¶Aerodynamicist, Rolls-Royce plc. and visiting researcher, Propulsion Engineering Centre, Cranfield University
‖Installation Aerodynamics Specialist, Rolls-Royce plc.

(T_t) inflow profiles at the bypass duct inlet. The combined design space consisted of 17 geometric and aerodynamic design variables which were sampled with 935 points. The combined optimisation of exhaust geometry and inflow characteristics benefited the performance compared with a configuration with fixed inflow conditions. The combined optimisation increased the velocity coefficient (C_v) by 0.13%, 0.075% and 0.19% relative to fixed-inflow optimisations for tip, mid and hub-loaded fan OGV exit profiles, respectively. Another application of the same methodology [10] targeted the optimisation of bypass nozzle after-body geometries for Very High Bypass Ratio (VHBR) turbofans. The research studied the use of conical and curved bypass nozzle after-bodies as well as the position of the ventilation nozzle (vent) on the after-body. It concluded that the position of the vent on the after-body is a key parameter that can modify the flow topology substantially. The aerodynamic impact of the after-body curvature was found to be dependent on the axial location of the ventilation nozzle. However, the use of curved after-bodies did not improve the aerodynamic performance of the system relative to conical designs.

The works of Goulos et al. [8–11] established a baseline approach for the optimisation of exhaust systems. However, the methodology relied on the acquisition of sufficient data to construct accurate response surface models. In addition, the definition of exhaust geometries required a great number of degrees of freedom and the CFD approach was based on fine meshes to enable fully resolved boundary layers, which would result in significant computational overheads. This made the methodology computationally expensive and not suitable for preliminary design processes where typically faster optimisation methods are required. In this context, novel techniques such as dimensionality reduction become of interest. Dimensionality reduction methods can identify the dominant parameters (feature selection) or define a new set of parameters that are combinations of the initial design space (feature extraction). With the application of dimensionality reduction methods, high-dimensional problems could be projected to lower dimensional design spaces. For example, Tejero et al. [13] used a dimensionality reduction based method [14] to optimise an aero-engine nacelle. It was found that the 32-dimensional design space of 3D nacelles could be projected into a reduced design space characterised by 2 degrees of freedom. This, in combination with a multi-fidelity methodology based on surrogate models [15], enabled the optimisation of three-dimensional nacelles on installed arrangements with the airframe.

This work expands the research of Goulos et al. [8–11] on exhaust optimisation and develops a more rapid methodology for the optimisation of exhaust systems using dimensionality reduction. The methodology addresses the key steps of aerodynamic shape optimisation. These include the parametrisation of separate-jet exhaust geometries, the computational assessment of exhaust designs, an optimisation method with CFD in-the-loop and a methodology to identify the design parameters that govern the exhaust performance.

II. Methodology

This work develops a framework for computationally efficient optimisations of exhaust systems. The methodology encompasses all the steps of aerodynamic shape optimisation. Methods for the parametrisation of exhaust geometries and computational assessment with CFD are integrated into different optimisation routines. The optimisation methods investigated include Response Surface Model based methods, CFD in-the-loop optimisation and dimensionality reduction.

A. Baseline propulsion system and operating conditions

The baseline configuration is a modern civil Ultra-High Bypass Ratio Engine (UHBR). The reference configuration includes a compact nacelle [16] and a separate-jet exhaust system [10] (Fig. 1). The exhaust system comprises the bypass nozzle (BP), the core nozzle (CR) and the ventilation nozzle (vent). The operating conditions are the mid-cruise conditions of a long range flight at an altitude of $h = 10668m$ and a flight Mach number of $M_\infty = 0.85$. The ambient conditions of static pressure (p_∞) static temperature (t_∞) and density (ρ_∞) are defined through the International Standard Atmosphere (ISA) model [17]. The engine cycle is based on the works of Goulos et al. [5]. Overall Pressure Ratio (OPR) and Turbine Entry Temperature (TET) were used by Goulos et al. [4, 5] to derive optimum values for Fan Nozzle Pressure Ratio ($FNPR \approx 2.2$) and Core Nozzle Pressure Ratio ($CNPR \approx 1.5$) on the basis of minimising Specific Fuel Consumption (SFC) at mid-cruise conditions. At cruise, the aero-engine system has a standard nominal thrust of 60kN ($F_N \approx 60kN$) [5] and a bypass ratio of $BPR > 15$ [5]. The baseline exhaust system geometry considered in this work is based on the UHBR aero-engine exhaust configuration used as starting point in other exhaust design works [8] (Fig. 1). The exhaust flow for the baseline configuration is characterised by a notable under expanded shock-expansion pattern within the bypass exhaust jet.

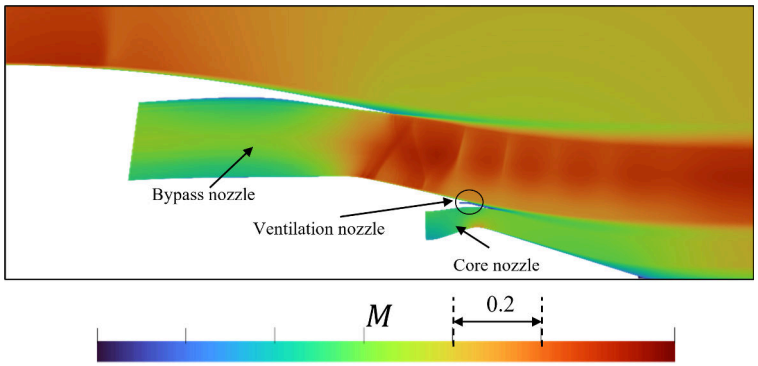

Fig. 1 Mach number distributions of the baseline exhaust design.

B. Exhaust geometry parametrisation

The geometries of separate-jet exhausts are parametrised with intuitive Class Shape Transformation functions (iCST) [4, 9, 10, 18–22] which relate the definition of exhaust aero-lines to a series of intuitive design parameters. Exhaust systems are characterised by 16 intuitive geometric parameters, or degrees of freedom (DoF). These encompass 6 parameters to define the bypass duct, 4 to represent the bypass nozzle, 3 for the after-body and 3 for the ventilation nozzle (Fig. 2). The bypass duct is defined with the radius of inner and outer control points ($R^{duct}_{BP_{in}}$, $R^{duct}_{BP_{out}}$) together with the radius (R^{in}_{cp}), slope ($\theta_{cp_{out}}$) and curvature radius (κ_{in}, κ_{out}) of the points at the charging plane (cp). The bypass nozzle is characterised with the charging-plane to exit area ratio (A_{ratio}), the wedge angle (θ_{wedge}), the length ratio (κ_{len}) and the straight line segment of the outer aeroline ($L^{straight}_{BP_{out}}$). The bypass nozzle after-body is defined with the core cowl (cc) boat tail angle (θ_{cc}) and length (L_{cc}) together with the core plug half-cone angle (θ_{plug}). The remaining parameters control the design and placement of ventilation nozzle (vent). The position of the vent over the core cowl is controlled with L^{Exit}_{vent}. The angle downstream of the vent is defined with a perturbation relative to the core cowl boat tail angle ($\Delta\theta_{vent}$). Finally, the ventilation nozzle also includes a straight-line segment on the inner aeroline that extends until its trailing edge ($L^{straight}_{vent}$).

C. Exhaust performance metrics

Within this work, the metric of interest is the velocity coefficient at infinity (C^{∞}_{v}, Eq. 1), which is the normalisation of the fully-expanded gauge stream force (F_{G_∞}) with the ideal propulsive force (IPF).

$$C^{\infty}_{v} = \frac{GPF}{IPF} \tag{1}$$

the fully-expanded gauge stream force (F_{G_∞}, Eq. 2) is calculated with the gauge stream forces (F_G) over the nozzle inlets ($F_{G_{BP}}$, $F_{G_{CR}}$, $F_{G_{Vent}}$) and wall forces (θ) over the walls inside the exhaust control volume (Fig. 3). These include the forces inside the bypass (θ_{BP}), core (θ_{CR}) and vent (θ_{vent}) as well as forces over the core cowl (θ_{cc}), core plug (θ_{plug}) and post-exit stream tube (θ_{post}). Gauge stream forces (F_G) and mass flows ($\dot{m}$) are calculated with numerical integration over the bypass (BP), core (CR) and ventilation nozzle ($vent$) and wall forces include pressure and viscous terms integrated over the different surfaces.

$$F_{G_\infty} = (F_{G_{BP}} + F_{G_{CR}} + F_{G_{Vent}}) - (\theta_{BP} + \theta_{CR} + \theta_{vent} + \theta_{CC} + \theta_{plug} + \theta_{post}) \tag{2}$$

The ideal propulsive force (Eq. 3) is calculated with the mass flows computed from the numerical solution ($\dot{m}^{CFD}$) and the ideal velocity (v^{id}). The ideal velocity is calculated assuming a perfectly expanded exhaust flow without total pressure losses and depends on the ratio of specific heats (γ), the universal gas constant (R), the total temperature at the nozzle inlet (T_t) and the nozzle pressure ratio ($NPR = P_t/p_\infty$)

$$IPF = \dot{m}^{CFD}_{BP} v^{id}_{BP} + \dot{m}^{CFD}_{CR} v^{id}_{CR} + \dot{m}_{vent} v^{id}_{vent} \tag{3}$$

$$v^{id} = \sqrt{\frac{2\gamma R T_t}{\gamma - 1}\left(1 - \left(\frac{1}{NPR}\right)^{\frac{\gamma-1}{\gamma}}\right)} \tag{4}$$

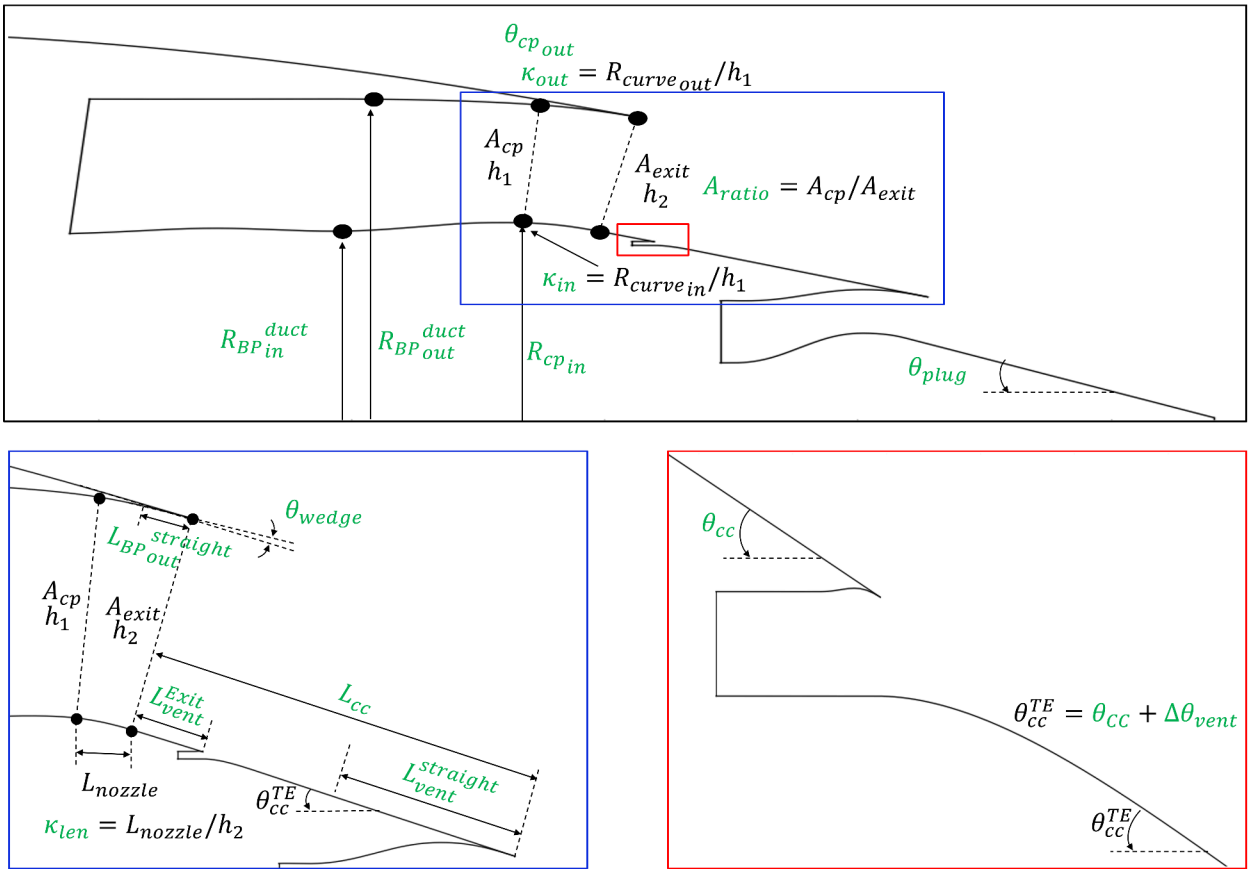

Fig. 2 Design parameters of a separate-jet exhaust systems. Parameters in green are directly specified and those in black are derived.

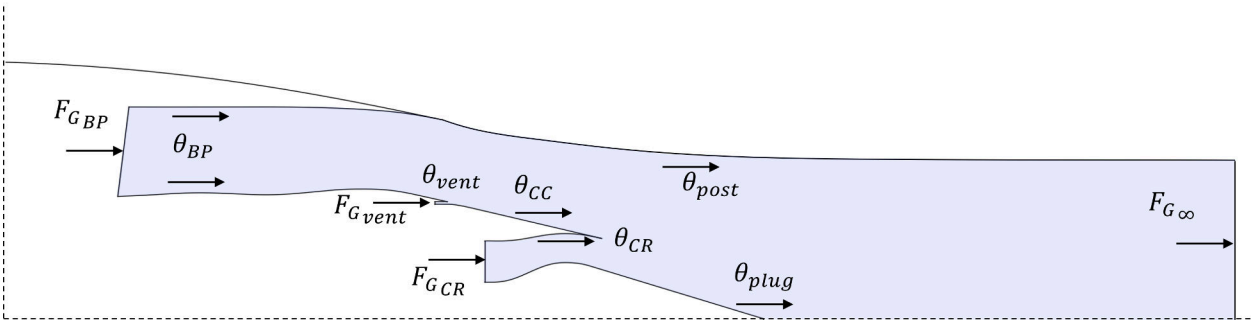

Fig. 3 Schematic of the forces acting over a separate-jet exhaust system

D. Computational assessment of exhaust systems

Computational fluid dynamics (CFD) methods are used to assess the exhaust system designs. The CFD method is based on the solution of the compressible Reynolds Averaged Navier Stokes (RANS) on two-dimensional axisymmetric domains. The CFD solver is density-based, implicit and steady-state [23]. In addition, the CFD approach is coupled with 2^{nd} order convective schemes and the $k-\omega$ SST turbulence model of Menter [24]. The dynamic viscosity of the fluid is calculated with the Sutherland's law [25] and the heat capacity at constant pressure (C_p) is assumed to vary with the static temperature according to an 8^{th} order polynomial [26].

The fan face is treated as pressure outlet that prescribes a mass flow to ensure a target mass flow capture ratio (MFCR). Bypass, core and vent nozzle inlets are modelled as total pressure inlets with the values specified according to their pressure ratio. The inflow condition is set as pressure far field with $M_\infty = 0.85$, static pressure and temperature that are set according to the International Standard Atomosphere (ISA) [17] at the target altitude. Computational grids are structured and ensure sufficient refinement in the regions of interest in the flow. These include near wall refinements for boundary layer resolution and refinements around the exhaust jet. The standard meshing approach targets a y^+ of approximately 1 on all non-slip walls and has approximately 800×10^3 cells. A grid independence analysis was carried out and reported by Goulos et al. [11] where the Grid Convergence Index (GCI) for the velocity coefficient was approximately 0.058%.

The meshing approach with $y^+ < 1$ and 800×10^3 cells is computationally expensive to use in the optimisation process. In an optimisation, many hundreds of exhausts designs are assessed. For this reason, faster computational approaches are required for preliminary design and optimisation. In this context, coarser meshes were developed to guide the optimisation process. These grids are configured with $y^+ \approx 50$ near the wall and use wall functions to reduce the amount of cells required to treat the boundary layer. Three coarser meshes with $y^+ \approx 50$ and different levels of refinement were developed. These had $\approx 380 \times 10^3$, $\approx 250 \times 10^3$ and $\approx 140 \times 10^3$ cells. To assess the coarse meshes, CFD solutions of 150 different exhaust designs (N=150) obtained with the different grids were compared with results of the baseline process ($y^+ < 1$ and 800×10^3 cells) for the same exhaust database. The meshes were evaluated in terms of Root Mean Squared Deviation (RMSD) (Eq. 5) across the database of 150 designs ($N = 150$) (Table 1).

$$RMSD(C_v^\infty) = \sqrt{\frac{\sum_{i=1}^{N}(C_{v_{baseline_i}}^\infty - C_{v_{coarse_i}}^\infty)^2}{N}} \tag{5}$$

Table 1 Summary of the different grids assessed. The standard deviation (2σ) is expressed relative to a linear regression line and is a measure of the random error of each meshing approach.

Mesh	Cell count	y^+	computational cost	$RMSD(C_v^\infty)$	$2\sigma(C_v^\infty)$
Baseline	$800k$	< 1	1	0.000%	0.000%
Coarse 1	$380k$	≈ 50	0.70	0.045%	0.023%
Coarse 2	$250k$	≈ 50	0.50	0.048%	0.024%
Coarse 3	$140k$	≈ 50	0.25	0.054%	0.027%

The coarse mesh with 140k (Coarse 3, Table 1) cells and a non-dimensional wall distance of $y^+ = 50$ reduced the computational time required to assess the database of 150 design by approximately 4 times relative to the baseline CFD approach. However, the reduction of computational time comes at a cost of increased uncertainty relative to the baseline method. For C_v^∞, the RMSD of the $140k$ cell mesh is of approximately 0.05% (Table 1). However, this value represents the absolute error of the coarse method. For this work, it is more relevant to quantify the error by means of bias and random terms. This was assessed in terms of linear correlation between methods and standard deviation ($\pm 2\sigma$) relative to the linear correlation (Fig. 4). It was found that the coarse mesh could approximate the variation of the results of the finer mesh approach within the designs space with a standard deviation of $\pm 0.027\%$ in C_v^∞ (Fig. 4). This result implies that an optimisation using coarse meshes would potentially guide the process to the same region of the design space. For this reason, the meshing approach with $140k$ cells and $y^+ \approx 50$ is used to guide the optimisation process. Although the optimisations are driven by the CFD method based on coarser meshes, the optimum designs are always evaluated with the standard meshing approach with $y^+ < 1$ and 800×10^3 cells.

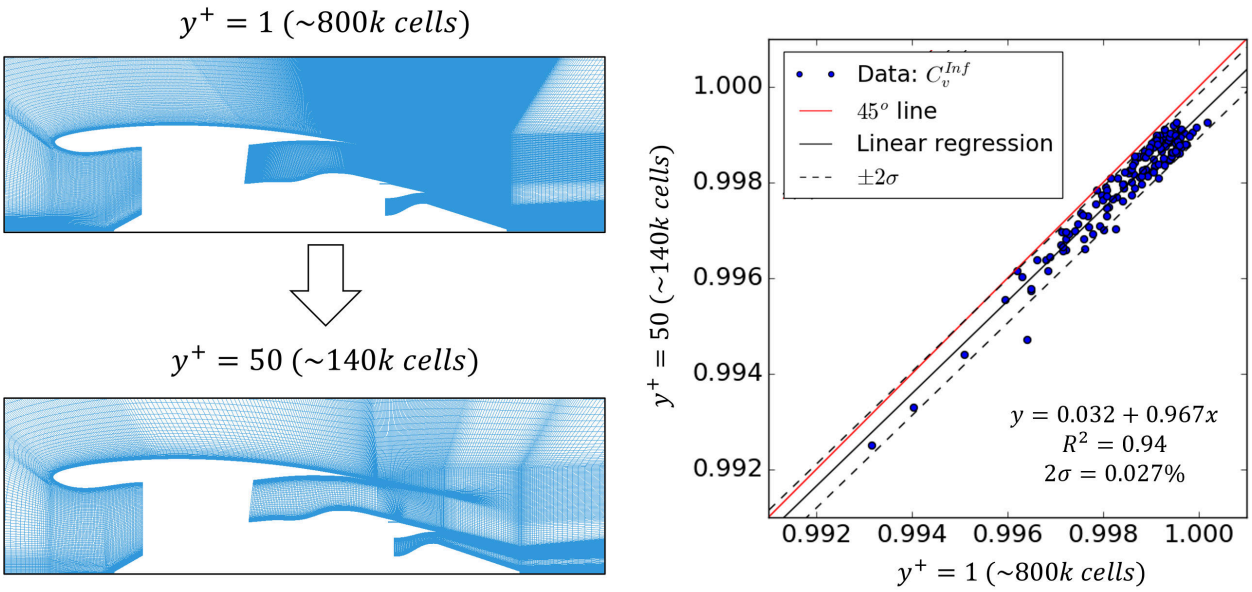

Fig. 4 Verification of the coarse mesh approach for the prediction of C_v^{∞}.

E. Optimisation methods

The optimisation of exhaust systems targeted the maximisation of C_v^{∞}. The optimisation started with an initial database of exhaust designs obtained with a Latin Hypercube Sampling (LHS) approach [12]. After that, the process was maintained during several generations until convergence. The optimum design was always evaluated with the CFD approach based on fine meshes and resolved boundary layers.

The different methods for exhaust optimisation include Response Surface Model (RSM) based methods and CFD in-the-loop methods. In a CFD in-the-loop approach, all designs throughout the optimisation process are evaluated with CFD. The is done using coarse meshes and wall functions to minimise the computational time. In a RSM based approach, an RSM is formulated from the initial database of exhaust designs and it is used as surrogate model for objective function evaluation. The RSMs used in this work are based on Gaussian Regression Process (Kriging, [27, 28]) and were configured with an absolute exponential correlation function and a quadratic regression function and a nugget value of $1e^{-7}$. This combination of parameters had the best possible response of the system and was verified for the prediction of an independent dataset.

1. Optimisation algorithms

One key aspect to a computationally effective optimisation process is the selection of a fast-converging optimisation algorithm. For this reason, three different evolutionary optimisation algorithms were considered. These are the Original Multi-Objective Particle Swarm Optimisation (OMOPSO) [29, 30], the Non-dominated Sorting Genetic Algorithm (NSGAII) [31] and the Indicator-Based Evolutionary Algorithm (IBEA) [32]. To test the performance of the optimisers, an analytical multi-objective function was selected for the optimisation, the Zitzler-Deb-Thiele's function N (Eq. 6 - 8) [33]. In this optimisation problem, both $f_1(x)$ and $f_2(x)$ are minimised.

$$Minimize = \begin{cases} f_1(x) = x_1 & 0 \le x_i \le 1 \\ f_2(x) = g(x)h(f_1(x), g(x)) & 1 \le i \le N \end{cases} \tag{6}$$

$$g(x) = 1 + \frac{9}{N-1}\sum_{i=2}^{N} x_i \tag{7}$$

$$f(f_1(x), g(x)) = 1 - \sqrt{\frac{f_1(x)}{g(x)}} \tag{8}$$

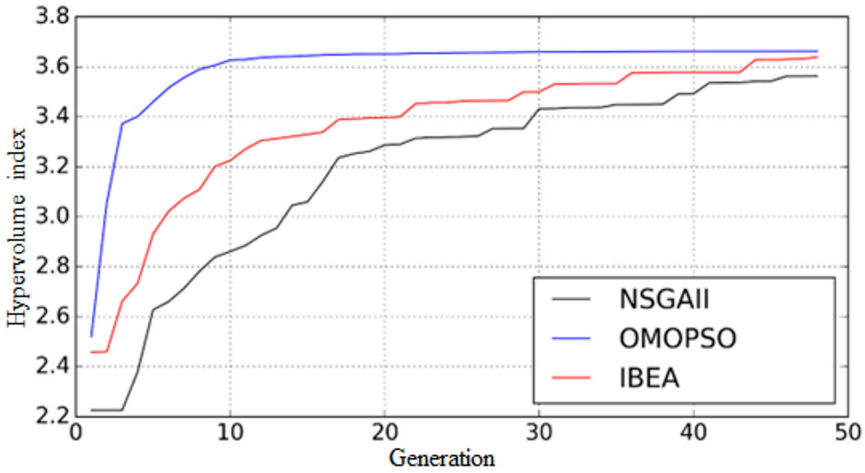

Fig. 5 Optimisation history of the NASGAII, OMOPSO and IBEA algorithms applied to Zitzler-Deb-Thiele's function N [33].

The three optimisation algorithms were tested on a 4D definition of the benchmark function (Fig. 5). The OMOPSO algorithm converged the optimisation in about 10 to 20 generations while NSGAII and IBEA required approximately 45 generations to reach a similar value of hypervolume index. Therefore, OMOPSO was selected for the rest of the work due to its fast convergence capabilities.

F. Dimensionality reduction with active subspaces

Active subspaces [14] is the methodology used for dimensionality reduction. The method aims to find a set of new variables (active variables) which are a linear combination of the full design space and can model the output of the system. The mathematical implementation of the method is based on the original derivation [14] and has been used in other aerodynamic optimisation works [13]. A brief description of the method is provided in this section.

The metric of interest f is a function of a vector $\mathbf{x}$ with n degrees of freedom. The n x n matrix $\mathbf{C}$ is the covariance of the gradient across the design space and can be expressed as in Eq. 9, where the gradient vector of ∇f is defined as in Eq. 10.

$$\mathbf{C} = E\left[\nabla f \nabla f^T\right] \tag{9}$$

$$\nabla f = \left[\frac{\partial f}{\partial x_1}, \frac{\partial f}{\partial x_2}, ..., \frac{\partial f}{\partial x_n}\right] \tag{10}$$

The matrix of gradient covariance ($\mathbf{C}$) is approximated with the snapshot method by using M samples (Eq. 11) in which ∇f_i is the gradient vector of the i sample (Eq. 12).

$$\mathbf{C} \approx \frac{1}{M}\sum_{n=1}^{M} \nabla f_i \nabla f_i^T \tag{11}$$

$$\nabla f_i = \nabla f x_i \tag{12}$$

After the approximation of the covariance matrix $\mathbf{C}$, an eigenvalue decomposition is applied (Eq. 13) where $\mathbf{W}$ is the eigenvectors matrix and $\wedge$ is a diagonal matrix with the eigenvalues. The values found in $\wedge$ are in descending order and contain the energy modes of the identified active variables. The matrix of the active subspace $\mathbf{U}$ can be built from $\mathbf{W}$. For example, the first column of $\mathbf{U}$ can be described as in Eq. 14 where $w_{1...n,1}$ refers to active variable weights from the first column of the matrix $\mathbf{W}$. To link the vector at the reduced dimensional space ($\mathbf{x_{as}}$) with the vector of the original space ($\mathbf{x}$), the matrix of the active subspace (U) is used (Eq. 15).

$$\mathbf{C} = \mathbf{W} \wedge \mathbf{W}^T \tag{13}$$

$$U_1 = \left[w_{1,1}, w_{2,1}, w_{3,1}, ..., w_{n,1}\right] \tag{14}$$

$$\mathbf{x} = U\mathbf{x_{as}} \tag{15}$$

The active subspace method was originally proposed as a methodology for feature extraction, whereby a new set of active variables is obtained from the original design space. However, the approach can also be applied to identify the dominant design variables of a given system (feature selection). This is achieved through the weights (w) of each design parameter in the active variables. Greater values of weights indicate higher levels of correlation between a design parameter and the metric of interest. However, in the active subspace method, each active variable is a linear combination of all the design parameters that constitute the design space. Therefore each design parameter has n number of weights associated, where n is the number of active variables. In order to extract a unique weight for each design parameter (W_k), the weights of the parameter in each active variable are scaled with the eigenvalue associated to that active variable ($EigV$) following equation 16. This scaling process allows the derivation of a ranking of importance of the design variables which can be used to identify the dominant parameters.

$$W_k = \sum_{i}^{n} \frac{W_{ik} EigV_i}{\sum_j^n EigV_j} \tag{16}$$

III. Results and discussion

A. Optimisation of dual separate jet exhaust systems with Response Surface Models

The baseline optimisation methodology is the same as in previous exhaust optimisation works [4, 10, 11]. It encompasses the maximisation of C_v^∞ for a fully defined exhaust system with 16 geometric design variables. The optimisation was guided with an RSM that was constructed with an exhaust dataset compiled with fine mesh CFD results (800k cells mesh, $y^+ = 1$). The dataset was generated with the Latin Hypercube Sampling method (LHS) and consisted of 60 designs per number of degrees of freedom ($N_S/nDOF = 60$), similar to previous works [11]. This resulted in a total of 960 exhaust designs. This method identified an optimum that improved the exhaust C_v^∞ by 0.06% relative to the baseline configuration. Although the method could identify a design with benefit in C_v^∞ relative to the baseline approach, the use of fine meshes and resolved boundary layers to generate the design database lead to substantial computational costs. For this reason, faster optimisation methods based on coarse meshes, CFD in-the-loop and with dimensionality reduction are investigated in the following sections.

B. Optimisation of dual separate jet exhaust systems with CFD in-the-loop

To improve the computational efficiency of exhaust design, CFD in-the-loop based optimisations guided with coarse meshes (140k cells) and wall functions were considered. However, the initial population ($Ns/nDOF$) and population per generation ($Ng/nDoF$) ratios in the optimisation also need to be carefully tuned to achieve maximum computational efficiency. The effects of the population ratios were investigated to determine the most suitable combination for a 16 DoF optimisation with CFD in-the-loop, coarse meshes and wall functions. The population ratios investigated comprised initial population ratios of $Ns/nDoF = 25$ and 50 with populations per generation of $Ng/nDOF = 3$ and 5 (Table 2). A total of 4 optimisations with different combinations of sampling ratios were investigated. All optimisations were stopped when the benefit increase over the previous 10 generations was lower than the method random error ($2\sigma = 0.027\%$, Fig. 4).

The best optimisation strategy was configured with $Ns/nDOF = 50$ and $Ng/nDOF = 3$ (CFD-2, Table 2). With these settings, the ΔC_v^∞ relative to the baseline configuration was of the order of 0.075%. This is within 0.01% of the design that resulted from the baseline optimisation with fine meshes and RSM. A difference in C_v^∞ of 0.01% is within the CFD uncertainty. Therefore the method can identify a design with similar performance relative to the baseline optimisation method but 2.7 times faster. The optimisation process was able to identify and mitigate adverse aerodynamic features (Fig. 6). For example, the baseline design exhibits shocks and expansion fans at the bypass nozzle exit plane, which indicate that the bypass flow is under-expanded. The under-expanded flow characteristics at the nozzle exit are mitigated in the optimum design. This is the result primarily of a reduced curvature at the inner aeroline of the bypass nozzle charging plane and an upstream placement of the ventilation nozzle (Fig. 6).

Table 2 Summary of exhaust optimisations with 16 design variables. The velocity coefficient is expressed relative to the baseline design (ΔC_v^∞) and was evaluated with the fine mesh approach.

Optimisation	nDOF	Method	Mesh	Ns/nDOF	Ng/nDOF	ΔC_v^∞	Comp. time
Baseline	16	RSM	800k, $y^+ = 1$	60	-	0.064%	1
CFD-1	16	CFD	140k, $y^+ = 50$	25	5	0.040%	0.27
CFD-2	16	CFD	140k, $y^+ = 50$	50	3	0.075%	0.37
CFD-3	16	CFD	140k, $y^+ = 50$	25	3	0.050%	0.39
CFD-4	16	CFD	140k, $y^+ = 50$	50	5	0.060%	0.51

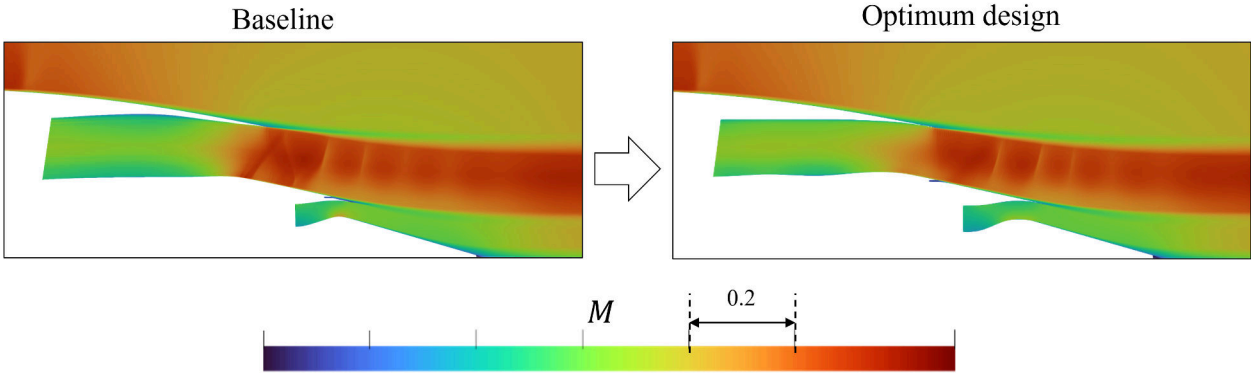

Fig. 6 Mach number distributions of the baseline (left) and optimum (right) designs.

In conclusion, the optimisation of exhaust systems with CFD in-the-loop, coarse meshes and wall functions can reach similar levels of exhaust performance as the baseline approach based on fine meshes and RSM approximately 2.7 times faster. However, to enable faster optimisations, the number of design variables required to characterise an exhaust system needs to be reduced.

C. Optimisation of exhaust systems with dimensionality reduction

It has been demonstrated that a CFD in-the-loop optimisation of exhaust systems based on coarse meshes and wall functions can reduce substantially the computational time relative to a baseline approach based on RSMs and fine CFD. To reduce the computational time further, the number of design variables required to characterise the exhaust performance needs to be reduced. This section investigates the application of the feature-selection method to the exhaust design space. This is done to identify the dominant design parameters for exhaust C_v^∞. Moreover, the dimensionality reduction method is coupled with several optimisations to further reduce computational time.

1. Identification of dominant exhaust design parameters

The feature selection methodology based on active subspaces identifies the dominant design parameters for exhaust performance (C_v^∞) (Fig. 7). Figure 7 represents the scaled weights of the different degrees of freedom ranked in order of importance. For this example, it is demonstrated that there are 7 dominant design parameters with a scaled weight approximately one order of magnitude greater than the remaining 9 (Fig. 7). Therefore, the exhaust performance could potentially be characterised with 7 design parameters. The dominant variables encompass the control of the bypass nozzle and after-body design, the placement of the ventilation nozzle and the control of the outer aeroline of the bypass duct. The rest of the design parameters have a reduced impact on C_v^∞.

The design variables that control the bypass nozzle flow expansion process were identified as dominant. This indicates that the performance of the exhaust system is governed by shock-losses in the bypass nozzle flow and that it could potentially be minimised with only 7 parameters. This starts within the bypass nozzle with the control of the inner

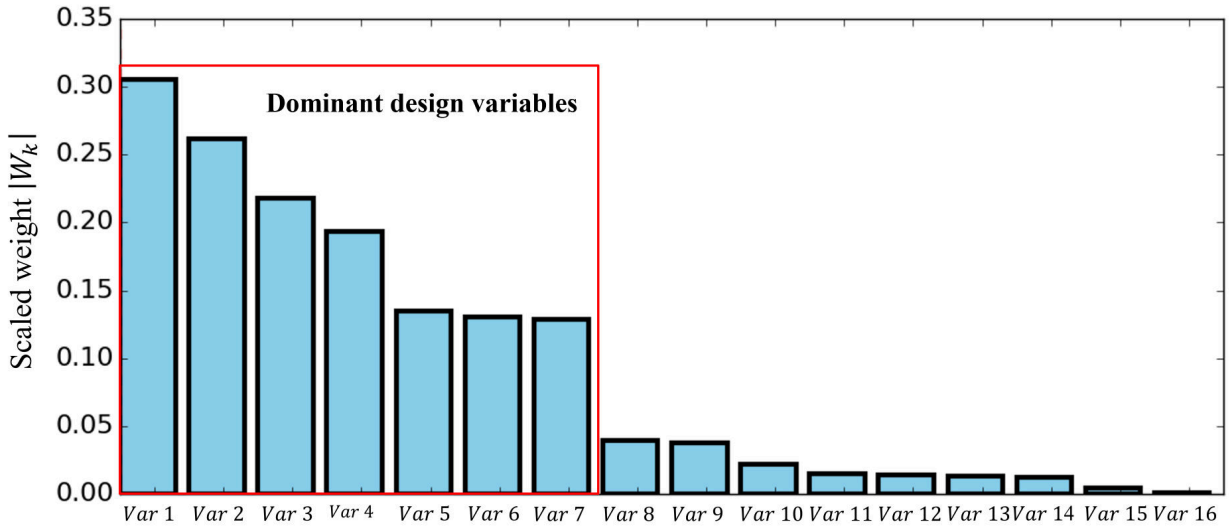

Fig. 7 Ranking of importance of the different exhaust design parameters and visual representation of the design spaces.

line curvature and continues to the after-body whereby with curvature control the shock-field potency can be minimised, therefore reducing the shock losses and improving performance. Moreover, the parameters that control the duct outer line are also identified as dominant. These parameters have an impact on total pressure loses within the duct.

To verify the Active Subspace methodology and find out the minimum data needed to derive the ranking of design variables different datasets were evaluated with coarse meshes and wall functions. Databases of $Ns/nDOF$ = 10, 15,25 and 50 were used to calculate the ranking. The same dominant design variables were obtained for $Ns/nDOF$ = 25 and 50 (Figure 8). Therefore, it was concluded that a population ratio of $Ns/nDOF$ = 25 was sufficient to capture the ranking of design variables. In addition, the ranking results obtained with coarse meshes and wall functions were compared with the results of the fine CFD approach ($Ns/nDOF$ = 60). It was found that the dominant design variables identified with the coarse mesh approach was consistent with the fine CFD approach (Figure 8).

2. Optimisation with sampling of the reduced design space

The first strategy for the optimisation with dimensionality reduction is outlined in Figure 9a. In this strategy, the complete design space (16 DoF) is initially assessed with coarse meshes and wall functions to derive the ranking information and identify the dominant design variables for optimisation. Moreover, the initial database is also used to create a Kriging RSM that is optimised for all 16 degrees of freedom. The Kriging RSM optimisation is used to identify suitable values for the non-dominant design parameters. Once the ranking of design parameters and suitable values for the non-dominant parameters are identified, a second database of exhausts is generated. In this case the LHS method is applied to the reduced design space of optimisation variables (dominant parameters). This is the resampling step (Figure 9a, in red), which is used as the initial dataset to start the CFD in-the-loop optimisation. Therefore, each optimisation with dimensionality reduction encompasses and initial database with 16 DoF and a reduced database only of the selected optimisation variables (dominant parameters).

This optimisation methodology is applied to study the effect of the number of optimisation variables. Exhausts were optimised with the 3, 5 and 7 most dominant design parameters and were compared with the results of the 16 DoF optimisation of the previous section (Figure 10, Table 3). For an increasing number of design variables, the optimum ΔC_v^{∞} tends asymptotically to the value of the 16 DOF optimisation (CFD-2, Table 3) (Figure 10). The optimisation with 7 design variables (DIM-1-WS) identified a candidate design with ΔC_v^{∞} of 0.06%, relative to the baseline design. This is approximately the same as the baseline optimisation method (Baseline, Table 3) and 0.014% lower than the full 16 DoF optimisation with CFD in-the-loop (CFD-2, Table 3). However, as the number of optimisation variables is reduced, the optimum C_v^{∞} is reduced substantially. With five optimisation variables (DIM-2-WS) the benefit in C_v^{∞} is reduced to 0.042%. With three, (DIM-3-WS) it is not possible to improve the performance of the baseline design (Table 3).

In terms of computational time, the CFD in-the-loop optimisation with 7 DoF (DIM-1-WS) is approximately 3.7

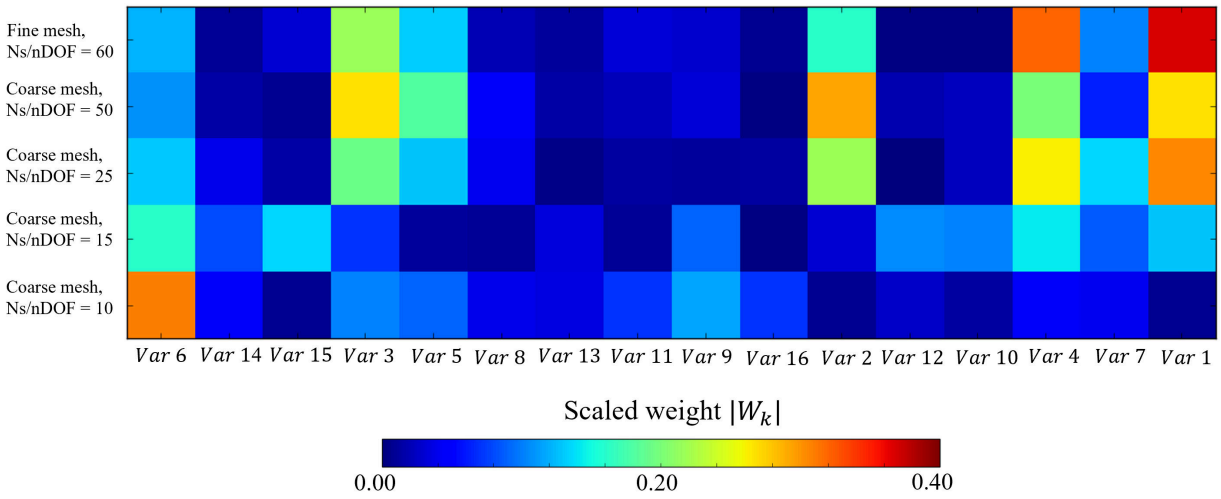

Fig. 8 Effect of the population ratio (Ns/nDOF) and CFD fidelity on the ranking of geometric design variables.

a. Optimisation with sampling of the reduced design space

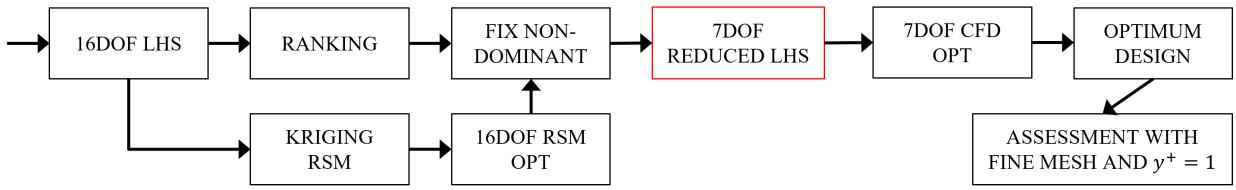

b. Optimisation without sampling of the reduced design space

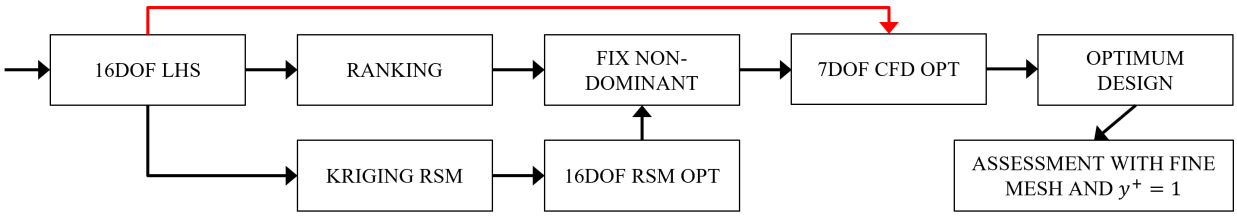

Fig. 9 Flow diagrams of the different optimisation methods with dimensionality reduction. (a) Method with a 2^{nd} exploration of the design space and (b) method without it.

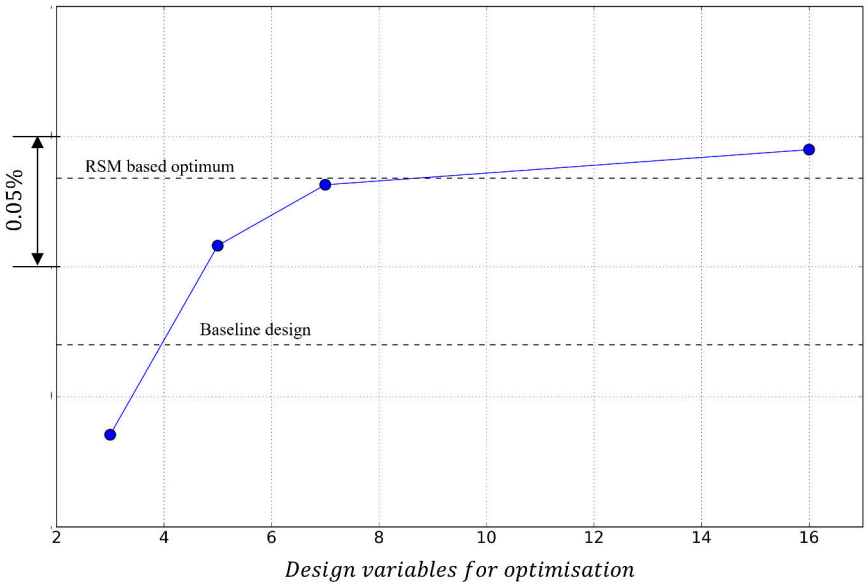

Fig. 10 Effect of the number of design parameters on the optimised C_v^∞. C_v^∞ is based on the evaluation of the optimum designs with fine meshes and $y^+ = 1$

Table 3 Summary of exhaust optimisations. The velocity coefficient is expressed relative to the baseline design (ΔC_v^∞) and was evaluated with the fine mesh approach.

Optimisation	nDOF	Method	Mesh	Ns/nDOF	Ng/nDOF	ΔC_v^∞	Comp. time
Baseline	16	RSM	800k, $y^+ = 1$	60	-	0.064%	1
CFD-2	16	CFD	140k, $y^+ = 50$	50	3	0.075%	0.37
DIM-1-WS	7	CFD	140k, $y^+ = 50$	25	5	0.061%	0.27
DIM-2-WS	5	CFD	140k, $y^+ = 50$	25	5	0.042%	0.24
DIM-3-WS	3	CFD	140k, $y^+ = 50$	25	5	-0.030%	0.17
DIM-4-WOS	7	CFD	140k, $y^+ = 50$	25	5	0.072%	0.22

times faster than the baseline optimisation method with fine CFD and RSMs (Table 3). This includes the time required for the initial (16 DoF) and reduced (7 DoF) explorations of the design space as well as the optimisation generations. Although the identification of the dominant variables required an initial database of 16 DOF, the results indicate that for an exhaust design style, subsequent optimisations with specific constraints could be undertaken with fewer variables to enable a quicker design process.

3. Optimisation without sampling of the reduced design space

It is demonstrated that UHBR aero-engine exhausts could be optimised with 7 geometric DOF. However, the method required an initial investigation of the design space to identify the dominant design parameters and a second exploration of the reduced set of design variables to start the optimisation. For this reason, the computational time of the method could be further improved if both explorations were combined. In this context, a second optimisation methodology based on CFD in-the-loop and dimensionality reduction is proposed (Fig. 9b). The philosophy of this method is to perform an initial exploration of the full design space with 16 DoF to identify the dominant design parameters and to use the same data to start the optimisation with dimensionality reduction. Therefore, this methodology removes the resampling step in which a second LHS is calculated for the reduced design space (Fig. 9).

The main assumption of the method is that a lower-dimensional optimisation can be started from a higher-dimensional

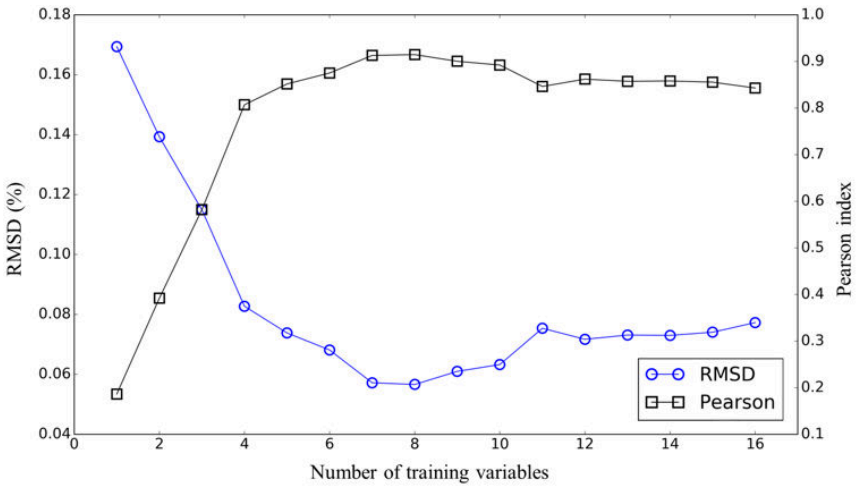

Fig. 11 RMSD and Pearson index of Kriging RSM trained with different number of geometric design variables selected from a 16 DoF database. The training database had a population ratio of $Ns/nDoF = 25$ and was evaluated with coarse meshes and wall functions.

LHS dataset. For example, a database of designs with 16 DoF could be used to start a CFD in-the-loop optimisation of the 7 dominant DoF. The key hypothesis is that the non-dominant design parameters do not have an impact on the exhaust performance. To verify the hypothesis, Kriging RSMs were trained with a 16 DoF exhaust database and tested with an independent dataset ($Ns/nDoF = 50$, coarse meshes and wall functions). However, non-dominant design variables were excluded from the training process. These were selected according to the ranking of importance (Fig. 7). Figure 11 demonstrates that the best performance of a Kriging RSM is achieved when the model is trained with 7 DoF (maximum Pearson index and minimum RMSD). This result indicates that the 9 non-dominant design parameters do not affect the exhaust C_v^∞ and may induce noise in the correlations of the design space. Therefore, a CFD in-the-loop optimisation for a reduced number of dominant degrees of freedom could be initialised from a database that also includes the non-dominant design parameters.

It is demonstrated that a process that targets the optimisation of the dominant design variables can be initialised from a more general database that also includes the non-dominant geometric parameters. For this reason, an exhaust optimisation process with a CFD in-the-loop, coarse meshes and wall functions is developed using the strategy outlined in Figure 9b. The method (DIM-4-WOS, Table 3) identified an exhaust configuration with $\Delta C_v^\infty = 0.072\%$ benefit relative to the reference design. This result is within 0.003% of the candidate design obtained with a 16 DOF optimisation (CFD-2). Moreover, the optimisation was approximately 4.4 times faster than the baseline optimisation approach based on RSM, fine meshes and resolved boundary layers (Table 3).

In terms of aerodynamics, all optimisations with dimensionality reduction mitigate the adverse under-expanded flow effects that characterise the baseline design. However, for the optimum obtained with 3 DoF (DIM3-WS), the flow is starting to separate near to core cowl trailing edge. This effect explains the reduction in C_v^∞ relative to the baseline design despite the mitigation of the under-expended flow features at the bypass nozzle. In addition, both designs obtained with 7 DoF (DIM1-WS and DIM4-WOS) exhibit Mach number distributions that are similar to the 16 DoF optimised design (CFD-2). These results indicate that the aerodynamics is sensitive to the most dominant design parameters but almost insensitive to the non-dominant ones. Therefore, it is confirmed that an optimisation process that targets the dominant design variables would be sufficient to capture the relevant aerodynamic effects.

For UHBR aero-engine exhausts, it is demonstrated that an optimisation process with dimensionality reduction can identify candidate designs with similar exhaust C_v^∞ and aerodynamics relative to a full dimensional optimisation. The methodology based on feature-selection identifies the dominant design variables in the design space and optimises only for those, which reduce computational cost.

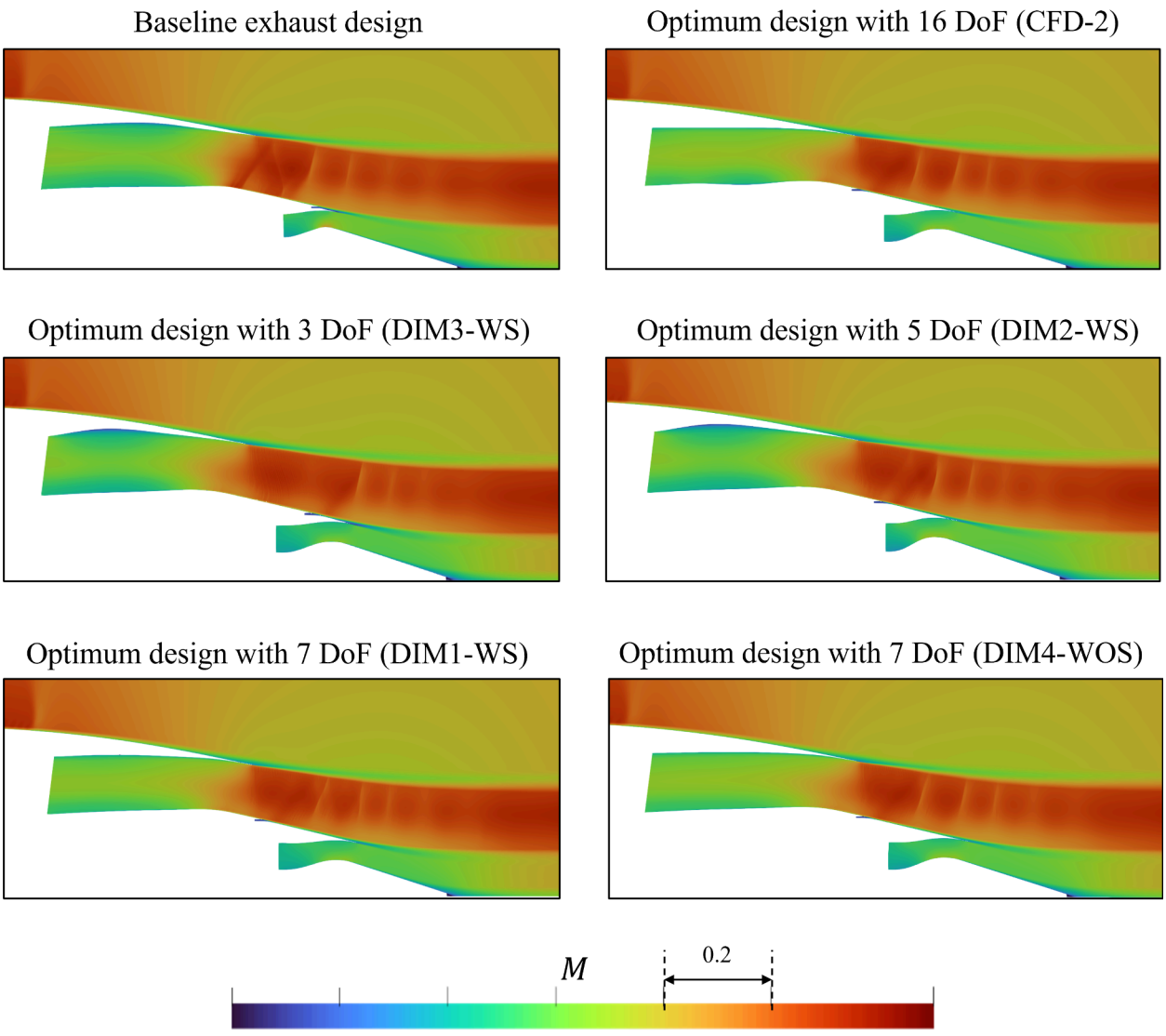

Fig. 12 Mach number contours for the baseline exhaust design and the different optimum configurations. It includes the optimum designs for a 16 DoF optimisation (CFD-2) and the optimum designs for optimisations with dimensionality reduction (DIM1-WS, DIM2-WS, DIM3-WS, DIM4-WOS). All design are evaluated with fine meshes and $y^+ = 1$.

IV. Conclusions

This work presents a novel methodology for the optimisation of UHBR exhaust systems with dimensionality reduction techniques. The optimisation is a single-objective methodology with CFD in-the-loop. The process is guided with a CFD approach that uses coarse meshes and wall functions to reduce the computational time of the optimisations.

The methodology is initially tested on a fully defined exhaust system with 16 design variables. The process is able to mitigate the adverse aerodynamic features of the baseline design and improves the nozzle velocity coefficient by 0.075%. Moreover the method is approximately 2.7 times faster than a baseline optimisation approach based on fine meshes and Response Surface Models.

A feature selection method based on active subspaces is developed and used to identify the parameters that govern the exhaust performance. Of the initial 16 design parameters, 7 were found to be important for the exhaust velocity coefficient. These variables control the bypass nozzle flow expansion process, which indicates that the performance of the exhaust system is governed by shock-losses in the bypass nozzle flow. Moreover, the method for dimensionality reduction was coupled with several optimisation processes. It was found that for an optimisation of the 7 dominant design variables, the optimum design had a similar velocity coefficient relative to the optimum obtained with 16 DoF. This approach reduced the computational time by 4.5 relative to the baseline approach.

Acknowledgments

This work has been partially funded by Rolls Royce plc. and Innovate UK.

Data availability

Due to commercial confidentiality agreements the supporting data is not available.

References

[1] Brich, N. T., "2020 Vision: The Prospects for Large Civil Aircraft Propulsion," *The Aeronautical Journal*, Vol. 104, No. 1038, 2000, pp. 347–352. doi:10.1017/S0001924000063971.

[2] Haselbach, F., "Next generation of large civil aircraft engines-concepts & technologies," *11 European Conference on Turbomachinery Fluid dynamics & Thermodynamics*, Madrid, Spain, 2015.

[3] Whurr, J., "Future Civil Aeroengine Architectures & Technologies," *10th European Conference on Turbomachinery, Guest lecture*, Lappeenranta, Finland, 2013.

[4] Goulos, I., Stankowski, T., Otter, J., MacManus, D., Grech, N., and Sheaf, C., "Aerodynamic Design of Separate-Jet Exhausts for Future Civil Aero-engines - Part I: Parametric Geometry Definition and Computational Fluid Dynamics Approach," *Journal of Engineering for Gas Turbines and Power*, Vol. 138, 2016. doi:10.1115/1.4032649.

[5] Goulos, I., Otter, J., Tejero, F., Hueso-Rebassa, J., MacManus, D., and Sheaf, C., "Civil turbofan propulsion aerodynamics: Thrust-drag accounting and impact of engine installation position," *Aerospace Science and Technology*, Vol. 111, 2021, p. 106533. doi:10.1016/j.ast.2021.106533.

[6] Hueso-Rebassa, J., MacManus, D., Goulos, I., and Tejero, F., "Design considerations of non-axisymmetric exhausts for large civil aero-engines," *AIAA Aviation and Aeronautics Forum and Exposition*, 2023.

[7] Hueso-Rebassa, J., "Design, Performance and Aerodynamics of Non-Axisymmetric Exhaust Systems for Civil Aero-Engines," PhD Thesis, Cranfield University, Cranfield, Bedfordshire, UK, 2022.

[8] Goulos, I., Otter, J. J., Stankowski, T., MacManus, D., Grech, N., and Sheaf, C., "Aerodynamic Design of Separate-Jet Exhausts for Future Civil Aero-engines - Part II: Design Space Exploration, Surrogate Modeling, and Optimization," *Journal of Engineering for Gas Turbines and Power*, Vol. 138, 2016. doi:10.1115/1.4032652.

[9] Goulos, I., Otter, J., Stankowski, T., MacManus, D., Grech, N., and Sheaf, C., "Design optimisation of separate-jet exhausts for the next generation of civil aero-engines," *Aeronautical Journal*, Vol. 122, 2018, pp. 1586–1605. doi:10.1017/aer.2018.95.

[10] Goulos, I., Stankowski, T., MacManus, D., Woodrow, P., and Sheaf, C., "Civil turbofan engine exhaust aerodynamics: Impact of bypass nozzle after-body design," *Aerospace Science and Technology*, Vol. 73, 2018, pp. 85–95. doi:10.1016/j.ast.2017.09.002.

[11] Goulos, I., MacManus, D., and Sheaf, C., "Civil turbofan engine exhaust aerodynamics: Impact of fan exit flow characteristics," *Aerospace Science and Technology*, Vol. 93, 2019. doi:10.1016/j.ast.2019.05.033.

[12] Olsson, A., Sandberg, G., and Dahlblom, O., "On Latin hypercube sampling for structural reliability analysis," *Structural Safety*, Vol. 25, 2003, pp. 47–68. doi:10.1016/S0167-4730(02)00039-5.

[13] Tejero, F., MacManus, D., Hueso-Rebassa, J., Sanchez-Moreno, F., Goulos, I., and Sheaf, C., "Aerodynamic optimisation of civil aero-engine nacelles by dimensionality reduction and multi-fidelity techniques," *International Journal of Numerical Methods for Heat and Fluid Flow*, 2022. doi:10.1108/HFF-06-2022-0368.

[14] Constantine, P. G., Dow, E., and Wang, Q., "Active subspace methods in theory and practice: applications to kriging surfaces," 2013. doi:10.1137/130916138.

[15] Hueso-Rebassa, J., Tejero, F., Otter, J., Goulos, I., and MacManus, D., "Multi-Fidelity Assessment of Exhaust Systems for Complete Engine-Aircraft Configurations," *Proceedings of Aerospace Europe Conference 2020 (AEC2020), 00337*, Bordeaux, France, 2020.

[16] Tejero, F., Goulos, I., MacManus, D., and Sheaf, C., "Effects of Aircraft Integration on Compact Nacelle Aerodynamics," Orlando, Florida, 2020. doi:10.2514/6.2020-2225, aIAA Scitech 2020 Forum, AIAA 2020-2225,1 Part F.

[17] ISO International Standard 2533-1975, "Standard Atmosphere First Edition," Tech. rep., ISO, Geneva, Switzerland, 1978.

[18] Kulfan, B., and Bussoletti, J., ""Fundamental" Parameteric Geometry Representations for Aircraft Component Shapes," *11th AIAA/ISSMO Multidisciplinary Analysis and Optimization Conference*, Vol. 1, American Institute of Aeronautics and Astronautics, Portsmouth, Virigina, 2006, pp. 547–591. doi:10.2514/6.2006-6948.

[19] Kulfan, B., "Recent extensions and applications of the 'CST' universal parametric geometry representation method," *The Aeronautical Journal*, Vol. 114, No. 1153, 2010, p. 157–176. doi:10.1017/S0001924000003614.

[20] Zhu, F., and Qin, N., "Intuitive class/shape function parameterization for airfoils," *AIAA Journal*, Vol. 52, 2014, pp. 17–25. doi:10.2514/1.J052610.

[21] Christie, R., Heidebrecht, A., and MacManus, D., "An automated approach to nacelle parameterization using intuitive class shape transformation curves," *Journal of Engineering for Gas Turbines and Power*, Vol. 139, 2017. doi:10.1115/1.4035283.

[22] Christie, R., Robinson, M., Tejero, F., and MacManus, D. G., "The use of hybrid intuitive class shape transformation curves in aerodynamic design," *Aerospace Science and Technology*, Vol. 95, 2019. doi:10.1016/j.ast.2019.105473.

[23] Ansys Inc, "ANSYS FLUENT User's Guide," Tech. rep., 2021.

[24] Menter, F. R., "Two-Equation Eddy-Viscosity Turbulence Models for Engineering Applications," *AIAA Journal*, Vol. 32, No. 8, 1994, pp. 1598–1605.

[25] Sutherland, W., "The Viscosity of Gases and Molecular Force," *Philosophical Magazine Series 5*, Vol. 36, 1893, pp. 507–531.

[26] Wood, G., "Gas Turbine Performance, P.P. Walsh and P. Fletcher, Blackwell Science, Osney Mead, Oxford OX2 0EL, UK. 1998. 628pp. Illustrated. £55." *The Aeronautical Journal (1968)*, Vol. 103, No. 1020, 1999, p. 126–126. doi:10.1017/S0001924000027834.

[27] Krige, D. G., "A statistical approach to some basic mine valuation problems on the Witwatersrand," *Journal of the Southern African Institute of Mining and Metallurgy*, Vol. 52, No. 6, 1951, pp. 119–139.

[28] V., P., Gommers, R., Oliphant, T. E., Haberland, M., Reddy, T., Cournapeau, D., Burovski, E., Peterson, P., Weckesser, W., Bright, J., van der Walt, S. J., Brett, M., Wilson, J., Millman, K. J., Mayorov, N., Nelson, A. R. J., Jones, E., Kern, R., Larson, E., Carey, C. J., Polat, I., Feng, Y., Moore, E. W., VanderPlas, J., Laxalde, D., Perktold, J., Cimrman, R., Henriksen, I., Quintero, E. A., Harris, C. R., Archibald, A. M., Ribeiro, A. H., Pedregosa, F., van Mulbregt, P., and SciPy 1.0 Contributors, "SciPy 1.0: Fundamental Algorithms for Scientific Computing in Python," *Nature Methods*, Vol. 17, 2020, pp. 261–272. doi:10.1038/s41592-019-0686-2.

[29] Sierra, M. R., and Coello, C. A. C., *Improving PSO-Based Multi-objective Optimization Using Crowding, Mutation and ?-Dominance*, 2005, pp. 505–519. doi:10.1007/978-3-540-31880-4_35, URL `http://link.springer.com/10.1007/978-3-540-31880-4_35`.

[30] Durillo, J. J., Garcia-Nieto, J., Nebro, A. J., Coello, C. A. C., Luna, F., and Alba, E., *Multi-Objective Particle Swarm Optimizers: An Experimental Comparison*, 2009, pp. 495–509. doi:10.1007/978-3-642-01020-0_39, URL `http://link.springer.com/10.1007/978-3-642-01020-0_39`.

[31] Deb, K., Pratap, A., Agarwal, S., and Meyarivan, T., "A fast and elitist multiobjective genetic algorithm: NSGA-II," *IEEE Transactions on Evolutionary Computation*, Vol. 6, 2002, pp. 182–197. doi:10.1109/4235.996017.

[32] Zitzler, E., and Kunzli, S., *Indicator-Based Selection in Multiobjective Search*, 2004, pp. 832–842. doi:10.1007/978-3-540-30217-9_84.

[33] Deb, K., Thiele, L., Laumanns, M., and Zitzler, E., "Scalable multi-objective optimization test problems," IEEE, 2002, pp. 825–830. doi:10.1109/CEC.2002.1007032, URL http://ieeexplore.ieee.org/document/1007032/.

2024-01-04

Design optimisation of separate-jet exhausts with CFD in-the-loop and dimensionality reduction techniques

Hueso-Rebassa, Josep

AIAA

Hueso-Rebassa J, MacManus DG, Tejero F, et al., (2024) Design optimisation of separate-jet exhausts with CFD in-the-loop and dimensionality reduction techniques. In: AIAA SCITECH 2024 Forum 2024, 8-12 January 2024, Orlando, FL, USA, Paper number AIAA 2024-1616
https://doi.org/10.2514/6.2024-1616